PHYSICAL REVIEW B **101**, 201404(R) (2020)

Rapid Communications

Low-temperature electron-phonon relaxation in Cu and Ag thin films

Shota Ono[*]

Department of Electrical, Electronic and Computer Engineering, Gifu University, Gifu 501-1193, Japan

(Received 1 March 2020; accepted 4 May 2020; published 11 May 2020)

The low-temperature electron-phonon (e-ph) relaxation near the surface of noble metals, Cu and Ag, is studied by using the density-functional theory approach. The appearance of the surface phonon mode can give rise to a strong enhancement of the Eliashberg function at low frequency ω. Assuming the Eliashberg function proportional to the square of ω in the low frequency limit, the e-ph relaxation time obtained from the surface calculations is shorter than that from the bulk calculation. The calculated e-ph relaxation time for the former is in agreement with a recent experiment for thin films.

DOI: 10.1103/PhysRevB.101.201404

Introduction. The electron-phonon (e-ph) interaction, one of the most important concepts in many-body theory, accounts for the superconductivity and the electrical resistivity [1,2]. Eliashberg function is a key to understand the details of the e-ph interaction in a variety of metals. For example, the integration of the weighted Eliashberg function results in the e-ph coupling constant that determines the superconducting transition temperature.

The e-ph coupling also plays an important role in nonequilibrium condition between electrons and phonons. The energy transfer dynamics is approximately described by the two-temperature model (TTM) for the electron temperature $T_{\rm e}$ and the phonon temperature $T_{\rm p}$ [3]. The temperature (T) relaxation time τ in the TTM is different between the high and the low-T limit. At high T, where the thermal energy is much larger than the Debye energy, τ is proportional to T. This model has been used in the field of ultrafast dynamics [4–6], while several models beyond the TTM have been proposed recently [7–9]. At low T, it crucially depends on the low frequency (ω) behavior of Eliashberg function: When the behavior ω^p with an integer p is assumed in the low ω limit, $\tau \propto T^{-p-1}$. For clean metals, $p = 2$ [10], while for dirty metals, the value of p is scattered [11–14]. It also depends on the dimension and the boundary condition in a complicated manner [15–17].

Notwithstanding the importance in the field of thermometry [18] and calorimetry [19–21] of nanoscale systems, the understanding of the low T e-ph relaxation is still under debate even for clean metals. The magnitude of τ can be related to the energy transfer rate $Q = \Sigma\Omega(T_{\rm e}^5 - T_{\rm ph}^5)$, where Ω is the volume of the metal and Σ is a parameter involving the e-ph coupling introduced in Ref. [10]. The magnitude of Σ evaluated within the deformation potential (DP) approximation has been found to be much smaller than that measured experimentally. This may be attributed to a lack of the Umklapp scattering contribution [10] and the nonspherical effect of the Fermi surface [15] in the DP model. However, a recent experiment has shown that the free-electron model can well describe the e-ph relaxation in Ag but not Cu [22]. The density-functional theory (DFT) approach enables us to calculate the Eliashberg function at low ω accurately and therefore to investigate τ at low T. However, to the best of our knowledge, such a DFT approach has yet to be applied to this issue.

At low T, the electron mean free path is long enough to be comparable to the sample size, allowing electrons to be scattered by surface phonons. In this paper, by performing DFT calculations, we investigate the low T e-ph relaxation near the surface as well as bulk of noble metals, Cu and Ag. Assuming the Eliashberg function proportional to ω^2, we show that the magnitude of τ for the surface model is much shorter than that for bulk and is in agreement with experiment [22]. We demonstrate that the electron-surface phonon interaction gives rise to an enhancement of the Eliashberg function at low ω as well as the magnitude of Σ and plays a key role to interpret the low T e-ph dynamics.

Basic concepts. The energy transfer rate of the total electron energy $E_{\rm e}$ per unit cell is derived from the Boltzmann equation for the electron and phonon distribution functions under the assumption: (i) The effects of the diffusion and the external forces are neglected; (ii) the electron and phonon quasiequilibrium is established at any time. Using the Sommerfeld expansion $E_{\rm e}(T_{\rm e}) = E_{\rm e}(0) + \gamma T_{\rm e}^2/2$ with $\gamma = 2\pi^2 N_{\rm F} N_{\rm c} k_{\rm B}^2/3$, the time ($t$) evolution of $T_{\rm e}$ is given by [3]

$$C_{\rm e}\frac{dT_{\rm e}}{dt} = -\Gamma(T_{\rm e}) + \Gamma(T_{\rm p}), \tag{1}$$

$$\Gamma(T) = 4\pi N_{\rm F} N_{\rm c}\int_0^{\omega_{\rm D}} d\omega(\hbar\omega)^2\alpha^2F(\omega)n_{\rm B}(\omega, T), \tag{2}$$

where $C_{\rm e} = \gamma T_{\rm e}$ is the specific heat of the electron, $N_{\rm F}$ is the electron density of states (DOS) per unit cell and per spin at the Fermi energy $\varepsilon_{\rm F}$, $N_{\rm c}$ is the number of unit cell, $\hbar$ is the Planck constant, $n_{\rm B}(\omega, T)$ is the Bose-Einstein function at temperature T, and $\omega_{\rm D}$ is the Debye frequency. The Eliashberg function $\alpha^2F(\omega)$ is given by

$$\alpha^2F(\omega) = \frac{1}{\hbar N_{\rm F} N_{\rm c}}\sum_{\alpha,\alpha',\boldsymbol{k},}\sum_{\beta,\boldsymbol{q}}\left|g^{\beta}_{\alpha,\alpha'}(\boldsymbol{k},\boldsymbol{q})\right|^2 \times\delta(\varepsilon_{\rm F} - \varepsilon_{\alpha\boldsymbol{k}})\delta(\varepsilon_{\rm F} - \varepsilon_{\alpha'\boldsymbol{k}+\boldsymbol{q}})\delta(\omega - \omega_{\beta\boldsymbol{q}}), \tag{3}$$

---

[*] shota_o@gifu-u.ac.jp

2469-9950/2020/101(20)/201404(5)

where $\varepsilon_{\alpha\boldsymbol{k}}$ is the single-particle electron energy with the wave vector $\boldsymbol{k}$ and the band index α, $\omega_{\beta\boldsymbol{q}}$ is the phonon frequency for the wave vector $\boldsymbol{q}$ and the branch index β, and $g^{\beta}_{\alpha,\alpha'}(\boldsymbol{k},\boldsymbol{q})$ is the matrix elements for the e-ph interaction Hamiltonian. The pth moment of $\alpha^2F(\omega)$ is defined as

$$\lambda\langle\omega^p\rangle = 2\int d\omega\alpha^2F(\omega)\omega^{p-1} \tag{4}$$

with an integer p. λ and $\lambda\langle\omega^2\rangle$ have been used as a measure of the strength of the e-ph coupling in metals.

At high T, where $n_{\rm B}(\omega,T)\simeq k_{\rm B}T/(\hbar\omega)$ holds, $\Gamma(T)$ is proportional to $\lambda\langle\omega^2\rangle$. At low T, where the thermal energy $k_{\rm B}T$ is much smaller than $\hbar\omega_{\rm D}$, numerical integration of Eq. (2) has to be performed by using an explicit expression of $\alpha^2F(\omega)$. In a clean metal, it is expected to be $\alpha^2F(\omega)\propto\omega^2$ at low ω, leading to $\Gamma(T)\propto T^5$. We thus define the e-ph coupling factor $\Sigma_{\rm low}$ as

$$\Sigma_{\rm low} = \frac{\Gamma_{\rm low}(T)}{N_{\rm c}\Omega_{\rm cell}T^5}, \tag{5}$$

where $\Omega_{\rm cell}$ is the volume of a unit cell.

From Eq. (1), the time evolution of $T_{\rm e}$ is written as

$$\frac{dT_{\rm e}}{dt} = -\frac{1}{\tau}(T_{\rm e}-T_{\rm p}), \tag{6}$$

where τ is defined by

$$\tau(T) = C_{\rm e}(T)\left(\frac{d\Gamma(T)}{dT}\right)^{-1} \tag{7}$$

under an assumption $T_{\rm e}\simeq T_{\rm p}\equiv T$ [22]. At low T, from Eq. (5), one obtains

$$\tau_{\rm low} = \frac{\gamma}{5\Sigma_{\rm low}N_{\rm c}\Omega_{\rm cell}T^3}\propto T^{-3}. \tag{8}$$

This means that when T is decreased, a very small amount of energy will be exchanged between the electron and the phonon due to small scattering phase space.

Computational details. We use DFT and density-functional perturbation theory implemented into QUANTUM ESPRESSO code [23] to obtain $N_{\rm F}$ and $\alpha^2F(\omega)$ in Eq. (2). The effects of exchange and correlation are treated within PBE-GGA [24]. The core electrons are treated within the ultrasoft pseudopotential method [25]. For Cu and Ag bulk calculations, the cutoff energies for the wave function $E_{\rm wf}$ and the charge density $E_{\rm cd}$ were set to 60 Ry and 600 Ry. For the calculation of $\alpha^2F(\omega)$ in Eq. (3), the dense k-point grid of $40\times40\times40$ (including k and $k+q$ points), the coarse k-point grid of $20\times20\times20$ (for constructing the charge density and the dynamical matrix), and the q-point grid of $10\times10\times10$ are used. In case of surface calculations, $E_{\rm wf}=90$ Ry and $E_{\rm cd}=900$ Ry were used. For the calculation of $\alpha^2F(\omega)$, the dense and coarse k-point grids of $24\times24\times1$ and $12\times12\times1$, respectively, and the q-point grid of $6\times6\times1$ are used, which are enough to study the phonon energy range of interest. The Marzari-Vanderbilt smearing [26] with a parameter of $\sigma=0.025$ Ry is used for all calculations.

The lattice constant is optimized to be $a_{\rm lat}=3.636$ Å and 4.154 Å for Cu and Ag bulk, respectively, where the total energy and forces are converged within 10^{-5} Ry and 10^{-4} a.u. For the surface calculations, where five or seven layers are considered, a vacuum layer between the surface is taken to be larger than 15 Å. The distance between the layers near the surface is shrunk by a few percent after the geometry optimization and thus the volume per atom decreases effectively. The optimized volume $\Omega_{\rm cell}$, the e-ph coupling constants, λ, $\lambda\langle\omega^2\rangle$, and $N_{\rm F}$ are listed in Table I. More details of DFT calculations on thin films are provided in Supplemental Material [27]. The values of λ for Cu and Ag bulk agree with other calculations [28,29]. The magnitude of $N_{\rm F}$ is almost proportional to the number of atoms in a unit cell.

TABLE I. The values of $\Omega_{\rm cell}$ (Å^3), λ, $\lambda\langle\omega^2\rangle$ (meV^2), $N_{\rm F}$ (states/eV/spin/unit cell), G (10^{-4}), $\Sigma_{\rm low}$ (GW/m^3/K^5), $\tau_{\rm low}(T=0.1{\rm K})$ (μs), and $\tilde{\gamma}=\gamma/\Omega_{\rm cell}$ (J/m^3/K^2).

	$\Omega_{\rm cell}$	λ	$\lambda\langle\omega^2\rangle$	$N_{\rm F}$	G	$\Sigma_{\rm low}$	$\tau_{\rm low}$	$\tilde{\gamma}$
Cu bulk	12.0	0.13	50.5	0.15	0.6	0.28	72.1	97.8
Cu (001) 5 layer	43.0	0.13	42.6	0.78	1.5	0.89	29.3	142.0
Cu (001) 7 layer	71.4	0.14	50.0	1.10	1.5	0.83	29.4	120.6
Cu (111) 7 layer	71.7	0.13	45.4	1.12	1.5	0.84	29.4	122.3
Ag bulk	17.9	0.14	24.4	0.14	2.0	0.55	21.6	61.2
Ag (001) 5 layer	70.9	0.15	20.8	0.68	6.0	2.06	7.2	75.1
Ag (001) 7 layer	106.7	0.15	22.2	0.97	6.0	1.95	7.2	71.2
Ag (111) 7 layer	106.9	0.14	21.2	0.97	6.0	1.95	7.2	71.0

Bulk. Figure 1 shows $\alpha^2F(\omega)$ for Cu and Ag. Below the phonon energy $\hbar\omega\simeq8$ meV for Cu and $\hbar\omega\simeq6$ meV for Ag, $\alpha^2F(\omega)$ shows a ω^2 behavior. The deviation from a ω^2 law at relatively low ω is attributed to a small number of Brillouin zone sampling, i.e., q mesh. Below, we thus use an analytical expression for low ω

$$\alpha^2F(\omega) = G\left(\frac{\hbar\omega}{E_0}\right)^2, \tag{9}$$

where $E_0=1$ meV and $\hbar\omega$ is the phonon energy in units of meV. Assuming Eq. (9), we calculate $\Gamma(T)$ in Eq. (2), $\Sigma_{\rm low}$ in Eq. (5), and $\tau_{\rm low}$ in Eq. (8). Table I lists the calculated G, $\Sigma_{\rm low}$, and $\tau_{\rm low}$ at $T=0.1$ K. The value of G for Ag is about three times larger than that for Cu. Accordingly, $\tau_{\rm low}$ of Ag is three times shorter than that of Cu. The size of $\Sigma_{\rm low}$ of Ag is larger

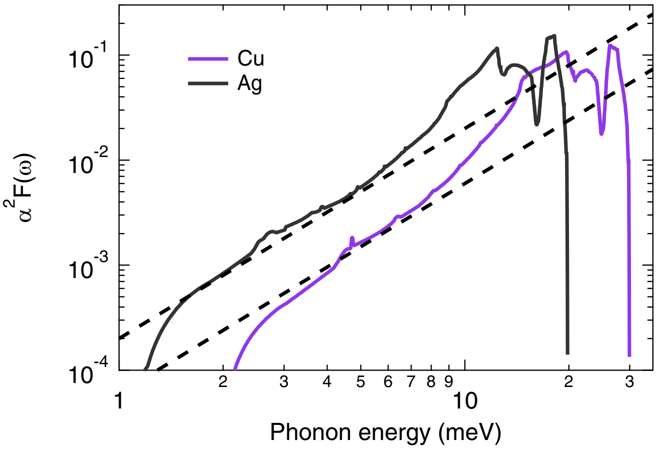

FIG. 1. The $\alpha^2F(\omega)$ of Cu and Ag bulk. The dashed lines indicate the curve of $\alpha^2F(\omega)\propto\omega^2$.

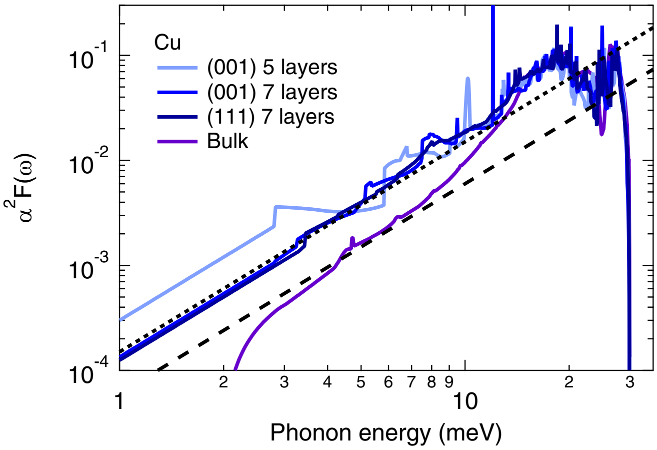

FIG. 2. The $\alpha^2F(\omega)$ of Cu thin films for (001) surface with five and seven layers and for (111) surface with seven layers.

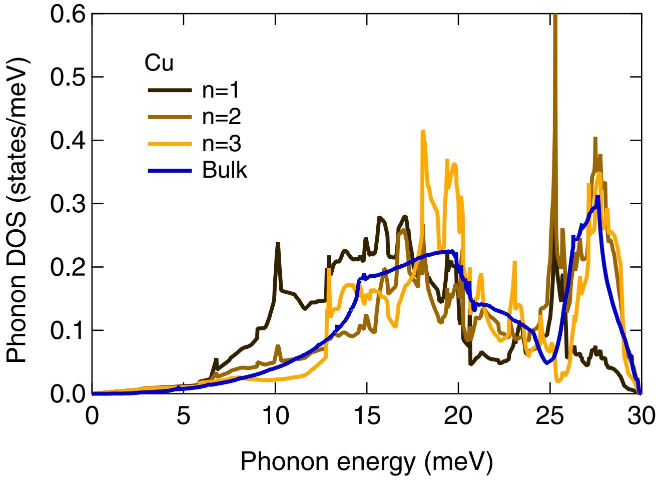

FIG. 4. The phonon DOS for Cu bulk and partial DOS for thin film with five layers. n denotes the layer number from the top ($n = 1$) to the middle ($n = 3$).

than that of Cu by a factor of two only, due to the difference of Ω_{cell} listed in Table I.

Surface. Figures 2 and 3 show $\alpha^2F(\omega)$ of Cu and Ag surfaces, respectively, for the cases of (001) surface with five and seven layers and (111) surface with seven layers. It is clear that the magnitude of $\alpha^2F(\omega)$ is enhanced at low ω, compared to the bulk case. The values of G, Σ_{low}, and τ_{low} at $T = 0.1$ K are also listed in Table I. The G and Σ_{low} in the surface are about three times larger than that in bulk. In accord with this enhancement, τ_{low} at $T = 0.1$ K becomes shorter than the bulk case: $\tau_{\text{low}} \simeq 30$ μs and 7 μs for Cu and Ag surfaces, respectively, almost independent of the film thickness and crystal surface.

The enhancement of $\alpha^2F(\omega)$ at low ω can be attributed to the appearance of the surface phonon mode, known as the Rayleigh mode, below the transverse acoustic phonon branch [30]. Figures 4 and 5 show the partial DOS for Cu and Ag thin films with five layers, respectively: n denotes the layer number from the top ($n = 1$) to the middle ($n = 3$). The partial DOS for $(6 - n)$th layer ($n = 1, 2$) is exactly the same as that for nth layer due to the presence of the inversion symmetry against the middle layer. The DOS for the bulk is also shown. The DOS of the middle and the second ($n = 2$) layers is similar to the bulk DOS at low ω. On the other hand, the magnitude of the DOS of the top layer is strongly enhanced below $\hbar\omega \simeq 15$ meV (Cu) and 9 meV (Ag) compared to the bulk DOS, which can be attributed to the surface phonon mode. Similar tendency is observed for the calculations with seven layers at (001) and (111) surfaces. Similar enhancement of the phonon DOS at low ω has been reported in DFT calculations for TiC [31] and NbC and TaC [32] thin films. It is natural to consider that this would modify the strength of $\alpha^2F(\omega)$ at low ω and therefore change the e-ph dynamics at low T.

Comparison to experiment. Recently, Viisanen and Pekola have investigated the e-ph relaxation dynamics at sub-Kelvin temperatures to extract the specific heat for Cu and Ag films [22]. First, they determined the value of the energy transfer rate Σ_{exp} ("exp" stands for experiment) from thermal conductance measurement: $\Sigma_{\text{exp}} \simeq 2$ GW/m^3/K^5 for Cu and $\Sigma_{\text{exp}} \simeq 3$ GW/m^3/K^5 for Ag. Next, they determined the relaxation time τ_{exp} of T_{e} by investigating the response against the

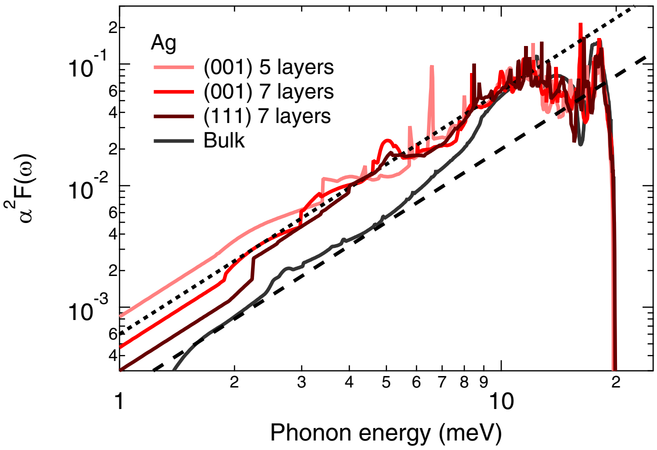

FIG. 3. The same as Fig. 2 but for Ag.

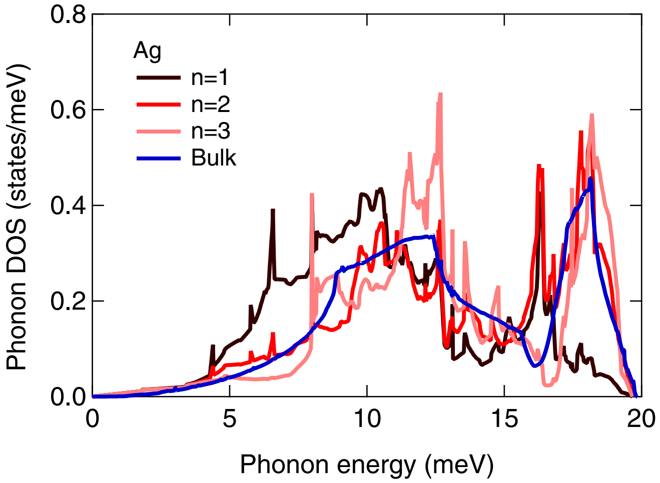

FIG. 5. Similar to Fig. 4 but for Ag.

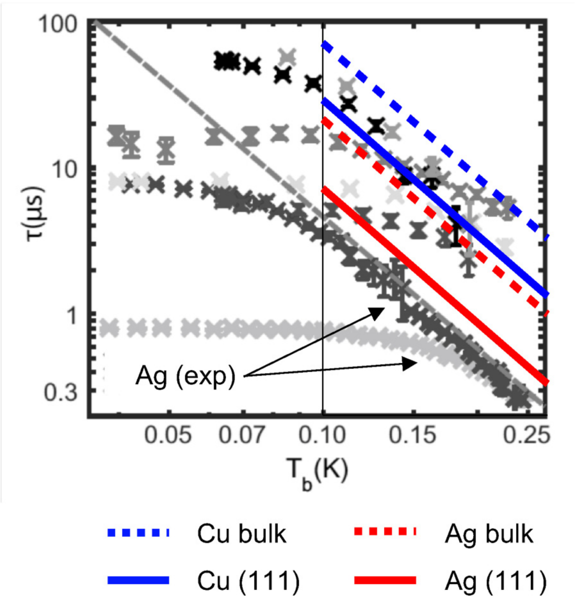

FIG. 6. The T dependence of $\tau_{\rm low}$ for Cu and Ag bulk (dashed) and (111) surface with seven layers (solid). Our results are compared to the experiment by Viisanen and Pekola, extracted from Ref. [22], where the plots for lower τs, indicated by arrows, are for Ag film, while the other plots are for Cu films. The different T dependence of τ in Ref. [22] is due to the use of different samples or measurements.

heating pulse: For example, $\tau_{\rm exp} \simeq 40$ μs for Cu and $\tau_{\rm exp} \simeq 3$ μs for Ag at $T = 0.1$ K. Assuming a relation $\tau_{\rm exp} \propto T^{-3}$ above $T = 0.1$ K, i.e., Eq. (8), they extracted the low-T specific heat $\tilde{\gamma}_{\rm exp}$ (the tilde is used to denote the specific heat per volume). They have found that the value of $\tilde{\gamma}_{\rm exp}$ in Ag film agrees with the free-electron estimate $\tilde{\gamma}_{\rm free} = 62.4$ J/m^3/K^2, while that in Cu films is anomalously larger than the estimate $\tilde{\gamma}_{\rm free} = 70.7$ J/m^3/K^2 by one order of magnitude. Below we interpret this experiment.

The calculated values of $\tilde{\gamma} = \gamma/\Omega_{\rm cell}$ are listed in Table I. Due to an effective decrease in the volume per atom, the value of $\tilde{\gamma}$ in thin films is larger than that in bulk. The agreement between $\tilde{\gamma}$ and $\tilde{\gamma}_{\rm exp}$ is good for Ag. However, the magnitude of $\tilde{\gamma}$ is not large enough to explain the experimental data of Cu [22]. When Eq. (8) is assumed, the discrepancy should be attributed to τ and Σ.

Figure 6 shows a comparison between $\tau_{\rm exp}$ [22] and $\tau_{\rm low}$ calculated for Cu and Ag bulk and (111) surface with seven layers. The value of $\tau_{\rm low}$ for bulk is much longer than that of $\tau_{\rm exp}$. With the surface effect, the value of $\tau_{\rm low}$ decreases and becomes the same order of magnitude of $\tau_{\rm exp}$. Similarly, the discrepancy between $\Sigma_{\rm low}$ and $\Sigma_{\rm exp}$ is reduced significantly, as listed in Table I. These indicate that the energy transfer at low T occurs through the electron-surface phonon scattering.

We analyze the discrepancy between the theory and experiment for τ and Σ in more detail. The value of $\Sigma_{\rm low}$ is a half and two thirds of $\Sigma_{\rm exp}$ for Cu and Ag surfaces, respectively. Such an underestimation would be due to a small value of G listed in Table I. It has been discussed that the effect of randomness can enhance the e-ph coupling [11,13]. By considering that the Cu sample used is polycrystalline [22], the magnitude of G in Cu would be more enhanced in the realistic situation. On the other hand, the value of $\tau_{\rm low}$ is shorter and longer than that of $\tau_{\rm exp}$ for Cu and Ag surfaces, respectively. The underestimated value of $\tau_{\rm low}$ in Cu is not explained by an enhancement of G. At present, we consider that the combined effect of the surface phonon and the grain boundary would be a key to resolve the discrepancy between the theory and experiment in a consistent way. In future work, we plan to perform DFT calculations on a supercell with large surface area that contains the grain boundary.

Conclusion. Using DFT calculations, we have calculated the Eliashberg function $\alpha^2F(\omega)$, the e-ph energy transfer rate $\Gamma_{\rm low}$, and the T dependence of $\tau_{\rm low}$ for the bulk and surfaces of Cu and Ag. We have shown that the surface effect is strong enough to modify the magnitude of $\alpha^2F(\omega)$ at low ω and $\Sigma_{\rm low}$, which can explain the low T electron relaxation dynamics observed in a recent experiment [22], while more detailed studies are required to obtain a consistent picture. We hope that this work would stimulate further study on the e-ph interaction for more realistic situations.

This study is supported by the Nikki-Saneyoshi Foundation.

---

[1] J. M. Ziman, *Electrons and Phonons* (Oxford University Press, New York, 1960).

[2] G. Grimvall, *The Electron-Phonon Interaction in Metals* (North-Holland, Amsterdam, 1981).

[3] P. B. Allen, Theory of Thermal Relaxation of Electrons in Metals, Phys. Rev. Lett. **59**, 1460 (1987).

[4] S. D. Brorson, A. Kazeroonian, J. S. Moodera, D. W. Face, T. K. Cheng, E. P. Ippen, M. S. Dresselhaus, and G. Dresselhaus, Femtosecond Room-Temperature Measurement of the Electron-Phonon Coupling Constant λ in Metallic Superconductors, Phys. Rev. Lett. **64**, 2172 (1990).

[5] V. V. Kabanov and A. S. Alexandrov, Electron relaxation in metals: Theory and exact analytical solutions, Phys. Rev. B **78**, 174514 (2008).

[6] M. Obergfell and J. Demsar, Tracking the Time Evolution of the Electron Distribution Function in Copper by Femtosecond Broadband Optical Spectroscopy, Phys. Rev. Lett. **124**, 037401 (2020).

[7] L. Waldecker, R. Bertoni, R. Ernstorfer, and J. Vorberger, Electron-Phonon Coupling and Energy Flow in a Simple Metal beyond the Two-Temperature Approximation, Phys. Rev. X **6**, 021003 (2016).

[8] P. Maldonado, K. Carva, M. Flammer, and P. M. Oppeneer, Theory of out-of-equilibrium ultrafast relaxation dynamics in metals, Phys. Rev. B **96**, 174439 (2017).

[9] S. Ono, Thermalization in simple metals: Role of electron-phonon and phonon-phonon scattering, Phys. Rev. B **97**, 054310 (2018).

[10] F. C. Wellstood, C. Urbina, and J. Clarke, Hot-electron effects in metals, Phys. Rev. B **49**, 5942 (1994).

[11] G. Bergmann, W. Wei, and Y. Zou, and R. M. Mueller, Nonequilibrium in metallic microstructures in the presence of high current density, Phys. Rev. B **41**, 7386 (1990).

[12] P. M. Echternach, M. R. Thoman, C. M. Gould, and H. M. Bozler, Electron-phonon scattering rates in disordered metallic films below 1 K, Phys. Rev. B **46**, 10339 (1992).

[13] A. Sergeev and V. Mitin, Electron-phonon interaction in disordered conductors: Static and vibrating scattering potentials, Phys. Rev. B **61**, 6041 (2000).

[14] J. T. Karvonen, L. J. Taskinen, and I. J. Maasilta, Observation of disorder-induced weakening of electron-phonon interaction in thin noble-metal films, Phys. Rev. B **72**, 012302 (2005).

[15] S.-X. Qu, A. N. Cleland, and M. R. Geller, Hot electrons in low-dimensional phonon systems, Phys. Rev. B **72**, 224301 (2005).

[16] F. W. J. Hekking, A. O. Niskanen, and J. P. Pekola, Electron-phonon coupling and longitudinal mechanical-mode cooling in a metallic nanowire, Phys. Rev. B **77**, 033401 (2008).

[17] S. Cojocaru and D. V. Anghel, Low-temperature electron-phonon heat transfer in metal films, Phys. Rev. B **93**, 115405 (2016).

[18] F. Giazotto, T. T. Heikkilä, A. Luukanen, A. M. Savin, and J. P. Pekola, Opportunities for mesoscopics in thermometry and refrigeration: Physics and applications, Rev. Mod. Phys. **78**, 217 (2006).

[19] J. P. Pekola and B. Karimi, Quantum noise of electron-phonon heat current, J. Low Temp. Phys. **191**, 373 (2018).

[20] F. Brange, P. Samuelsson, B. Karimi, and J. P. Pekola, Nanoscale quantum calorimetry with electronic temperature fluctuations, Phys. Rev. B **98**, 205414 (2018).

[21] B. Karimi, F. Brange, P. Samuelsson, and J. P. Pekola, Reaching the ultimate energy resolution of a quantum detector, Nat. Commun. **11**, 367 (2020).

[22] K. L. Visanen and J. P. Pekola, Anomalous electronic heat capacity of copper nanowires at sub-Kelvin temperatures, Phys. Rev. B **97**, 115422 (2018).

[23] P. Giannozzi, O. Andreussi, T. Brumme, O. Bunau, M. B. Nardelli, M. Calandra, R. Car, C. Cavazzoni, D. Ceresoli, M. Cococcioni, N. Colonna, I. Carnimeo, A. Dal Corso, S. de Gironcoli, P. Delugas, R. A. DiStasio, A. Ferretti, A. Floris, G. Fratesi, G. Fugallo, R. Gebauer, U. Gerstmann, F. Giustino, T. Gorni, J. Jia, M. Kawamura, H.-Y. Ko, A. Kokalj, E. Küçükbenli, M. Lazzeri, M. Marsili, N. Marzari, F. Mauri, N. L. Nguyen, H.-V. Nguyen, A. Otero-de-la-Roza, L. Paulatto, S. Poncé, D. Rocca, R. Sabatini, B. Santra, M. Schlipf, A. P. Seitsonen, A. Smogunov, I. Timrov, T. Thonhauser, P. Umari, N. Vast, X. Wu, and S. Baroni, Advanced capabilities for materials modelling with Quantum ESPRESSO, J. Phys.: Condens. Matter **29**, 465901 (2017).

[24] J. P. Perdew, K. Burke, and M. Ernzerhof, Generalized Gradient Approximation Made Simple, Phys. Rev. Lett. **77**, 3865 (1996).

[25] D. Vanderbilt, Soft self-consistent pseudopotentials in a generalized eigenvalue formalism, Phys. Rev. B **41**, 7892 (1990).

[26] N. Marzari, D. Vanderbilt, A. De Vita, and M. C. Payne, Thermal Contraction and Disordering of the Al(110) Surface, Phys. Rev. Lett. **82**, 3296 (1999).

[27] See Supplemental Material at http://link.aps.org/supplemental/10.1103/PhysRevB.101.201404 for computational details of DFT calculations on thin films.

[28] S. Y. Savrasov and D. Y. Savrasov, Electron-phonon interactions and related physical properties of metals from linear-response theory, Phys. Rev. B **54**, 16487 (1996).

[29] A. Giri, J. T. Gaskins, L. Li, Y.-S. Wang, O. V. Prezhdo, and P. E. Hopkins, First-principles determination of the ultrahigh electrical and thermal conductivity in free-electron metals via pressure tuning the electron-phonon coupling factor, Phys. Rev. B **99**, 165139 (2019).

[30] L. D. Landau and E. M. Lifshitz, *Elasticity Theory* (Pergamon, New York, 1986).

[31] S. Bağcı, T. Kamis, H. M. Tütüncü, and G. P. Srivastava, *Ab initio* calculation of phonons for bulk TiC and TiC(001)(1 × 1), Phys. Rev. B **80**, 035405 (2009).

[32] S. Bağcı, H. M. Tütüncü, S. Duman, and G. P. Srivastava, Surface phonons on the NbC(001) and TaC(001) surfaces, Phys. Rev. B **85**, 085437 (2012).